Microscopic Kinetics Pathway of Salt Crystallization in Graphene Nanocapillaries

Lifen Wang [1,2,*,†] Ji Chen [3,*] Stephen J. Cox [4,*,‡] Lei Liu,[5,§] Gabriele C. Sosso [6] Ning Li,[7,8]
Peng Gao,[7,8] Angelos Michaelides [4,9,10] Enge Wang,[1,2,7,11,12] and Xuedong Bai [1,2,13,‖]

[1]*Beijing National Laboratory for Condensed Matter Physics, Institute of Physics, Chinese Academy of Sciences, Beijing 100190, China*
[2]*Songshan Lake Laboratory for Materials Science, Dongguan 523000, China*
[3]*School of Physics and the Collaborative Innovation Center of Quantum Matters, Peking University, Beijing 100871, China*
[4]*Yusuf Hamied Department of Chemistry, University of Cambridge, Lensfield Road, Cambridge CB2 1EW, United Kingdom*
[5]*School of Materials Science and Engineering, Peking University, Beijing 100871, China*
[6]*Department of Chemistry and Centre for Scientific Computing, University of Warwick, Coventry CV4 7AL, United Kingdom*
[7]*International Center for Quantum Materials, School of Physics, Peking University, Beijing 100871, China*
[8]*Electron Microscopy Laboratory, School of Physics, Peking University, Beijing 100871, China*
[9]*Department of Physics and Astronomy, and Thomas Young Centre, University College London, London WC1E 6BT, United Kingdom*
[10]*London Centre for Nanotechnology, University College London, London WC1H 0AH, United Kingdom*
[11]*School of Physics, Liaoning University, Shenyang 110036, China*
[12]*Interdisciplinary Institute of Light-Element Quantum Materials and Research Center for Light-Element Advanced Materials, Peking University, Beijing 100871, China*
[13]*School of Physical Sciences, University of Chinese Academy of Sciences, Beijing 100190, China*

The fundamental understanding of crystallization, in terms of microscopic kinetic and thermodynamic details, remains a key challenge in the physical sciences. Here, by using *in situ* graphene liquid cell transmission electron microscopy, we reveal the atomistic mechanism of NaCl crystallization from solutions confined within graphene cells. We find that rock salt NaCl forms with a peculiar hexagonal morphology. We also see the emergence of a transitory graphitelike phase, which may act as an intermediate in a two-step pathway. With the aid of density functional theory calculations, we propose that these observations result from a delicate balance between the substrate-solute interaction and thermodynamics under confinement. Our results highlight the impact of confinement on both the kinetics and thermodynamics of crystallization, offering new insights into heterogeneous crystallization theory and a potential avenue for materials design.

Understanding and controlling the crystallization of materials from solution is of essential importance in various scientific and technological disciplines, including materials science, biology, geology, and atmospheric science [1,2]. In nature, complex phenomena such as cloud precipitation, biomineralization, and rock formation are associated with crystallization from solution [3], while industrially, solution-based methods offer a relatively simple and low-cost option for mass production [4]. This has motivated a large number of studies aimed at controlling the dynamics of nucleation, for example, the nucleation density, growth rate, and properties of crystals. For instance, by using additives, metals with finer grains, strengthened mechanical properties, and greater resistance to, e.g., salt damage, have been obtained in metallurgy [5,6].

Classical nucleation theory (CNT) gives a largely reasonable description of nucleation and crystallization. However, important questions remain, e.g., whether or not the stable phase nucleates from solution in a single- vs multistep fashion involving intermediate phases [7–12]. While still challenging, *in situ* graphene liquid cell (GLC)

imaging techniques provide a means to elucidate much needed microscopic insights into crystallization mechanisms [13]. Based on the assumption that graphene only interacts weakly with solution, the impact of the GLC on crystallization is often simply interpreted by effects due to reduced dimensionality and nanocapillary pressure, e.g., in studies of confined water [14–16]. However, a delicate balance between the substrate-solute interaction [17–19], the solute-solvent interaction, and thermodynamics under confinement [20] offers a new degree of freedom to modulate the crystallization pathway.

Conventional understanding suggests that NaCl follows a one-step classical nucleation pathway and grows into its conventional cubic rock salt structure (B1-NaCl) [21,22]. Using atoresolution *in situ* transmission electron microscopy (TEM), we reveal that, in a GLC, NaCl unexpectedly crystallizes into hexagonal-shaped crystallites, which predominantly expose their {110} facets instead of the conventional {100} facets. More surprisingly, a graphiticlike hexagonal NaCl phase (*h*-NaCl) [23] appears as an intermediate structure in the crystallization process, hinting

at a nonclassical nucleation pathway of NaCl in the GLC. Combined with density functional theory (DFT) calculations and control experiments, we highlight the importance of the interaction between the nascent crystallites and the graphene substrate, which could be considered as a kinetic approach to stabilize the hidden metastable phase and even as a means to effect nonclassical nucleation under confinement more generally.

Our experimental setup, comprising a quasi-two-dimensional graphene nanocell, is illustrated in Fig. 1(a). Given the higher electron scattering power of the saturated NaCl solution, we can identify the solution-encapsulated cells in the suspended TEM grid holes (see Fig. S1 in the Supplemental Material [24]). Figures 1(b), 1(d), and 1(e) show sequential high-resolution TEM images from one crystallization event (Video 1). The corresponding diffractogram is shown in Fig. 1(c), which demonstrates that the nanocrystal has a B1-NaCl structure along the {110}-zone axis (referred to as "{110}-B1-NaCl" hereafter). On-site electron energy loss spectroscopy (EELS) further confirms the NaCl composition (Fig. S2). The imaged nanocrystals show clear {100} and {111} facets with 120° angles, while {110} facets also evolve as transient side facets during the growth of this hexagonally shaped nanocrystal; as NaCl usually crystallizes into a cubic morphology, this observation comes as somewhat of a surprise. Moreover, this observation appears to be a feature of the GLC environment, as control experiments using open SiN_x cells produced B1 crystals with their usual cubic morphology (Fig. S3).

Although the stable B1 phase ultimately forms in our experiments, a different structural phase of NaCl is occasionally seen to form during the crystallization process. Figures 2(a)–2(d) show high-resolution TEM images along with the corresponding diffractograms. In the diffractograms, the graphene sheets with a rotation angle of 30° give rise to spots marked by outer white dashed circles (Fig. S4). In addition to these, six spots all with the same vector length from the center can be clearly recognized (yellow circles). These additional spots originate from the NaCl crystals, which is confirmed using EELS [Fig. 2(e)], and distribute evenly on the circle. Importantly, they differ from the first-order diffraction pattern of a "{111}-B1-NaCl" crystal; the {111} planes of B1-NaCl are hexagonally close packed so that {111}-B1-NaCl also has six equivalent first-order diffraction spots, but the vector length would be much larger. The sixfold symmetry of spots in reciprocal space thus indicates the formation of a hexagonal crystal structure of NaCl (h-NaCl), rather than the well-known B1 phase. Moreover, we carefully analyzed the relative angles between the graphene and the NaCl lattice and find the NaCl is not in registry with the graphene substrate.

Our assignment of this transient structure as h-NaCl is corroborated by an analysis of its facet growth dynamics. Figures 2(f)–2(h) show a sequence of TEM images from the longest-lived h-NaCl crystal. This allows us to track the growth of its facets (Videos 2 and 3). We find two predominant surfaces oriented 30° with respect to each other, as highlighted by the dashed lines. This is clearly distinct from the 120° angle seen for {110}-B1-NaCl, and the 90° angle expected for a typical B1 crystal exposing its {100} facets. The facet growth shown in Fig. 2 resembles other hexagonal materials such as graphene and hexagonal ice, where competition between the so-called zigzag and armchair edges is likely to evolve. Both the diffractograms and the facet growth dynamics are consistent with characterizing this transient structure as h-NaCl.

The observation of h-NaCl formation is intriguing and not expected based on conventional understanding of NaCl. To ascertain what role, if any, h-NaCl plays in the crystallization process, in Fig. 3 we present a sequence of TEM images depicting an entire crystallization event. Insets show the corresponding diffractograms. Initially, only a dark region corresponding to the encapsulated liquid is observed, and no sign of crystallization was seen [Fig. 3(a)]. In the early stages of crystallization, h-NaCl forms with a well-defined sixfold symmetry [Fig. 3(b)], which after approximately 3 s, begins to shrink [Fig. 3(c)], along with the emergence of B1 crystallites [Fig. 3(d)]. These B1 crystallites subsequently dominate the crystallization process, leading to the formation of a {110}-B1-NaCl nanocrystal showing well-marked facets with 120° angles [Fig. 3(e)]. From these images, we cannot
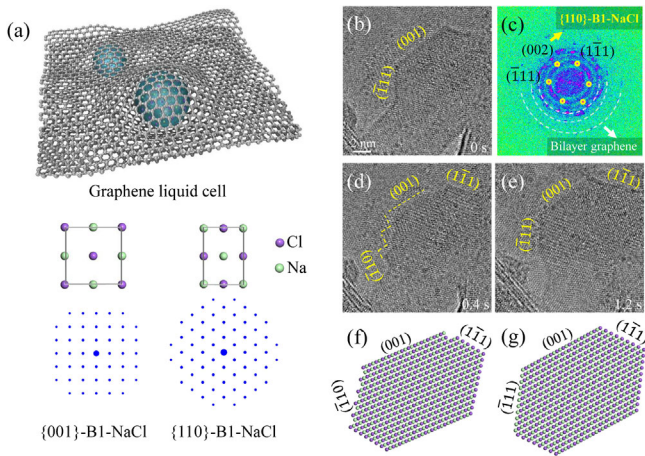

FIG. 1. Growth of the hexagonal-shaped B1-NaCl island. (a) Schematic of droplets encapsulated in a GLC, and the B1-NaCl crystal lattice viewed along the [001] and [110] crystallographic directions along with their corresponding diffraction patterns. (b) TEM image of a NaCl crystal grown in the GLC, showing low-index facets with 120° angles. (c) Corresponding diffractogram of the TEM image in (b), indicating NaCl oriented along [110]. (d),(e) Snapshots of the NaCl crystal growth process. While the (001) plane grows continuously, the ($\bar{1}$11) surface shows a sawtoothed plane composed of (001) and ($\bar{1}$10) facets, indicating that the layer-by-layer lateral growth of (001) and ($\bar{1}$10) facets dominate. (f),(g) Corresponding schematics of the TEM images shown in (d),(e).
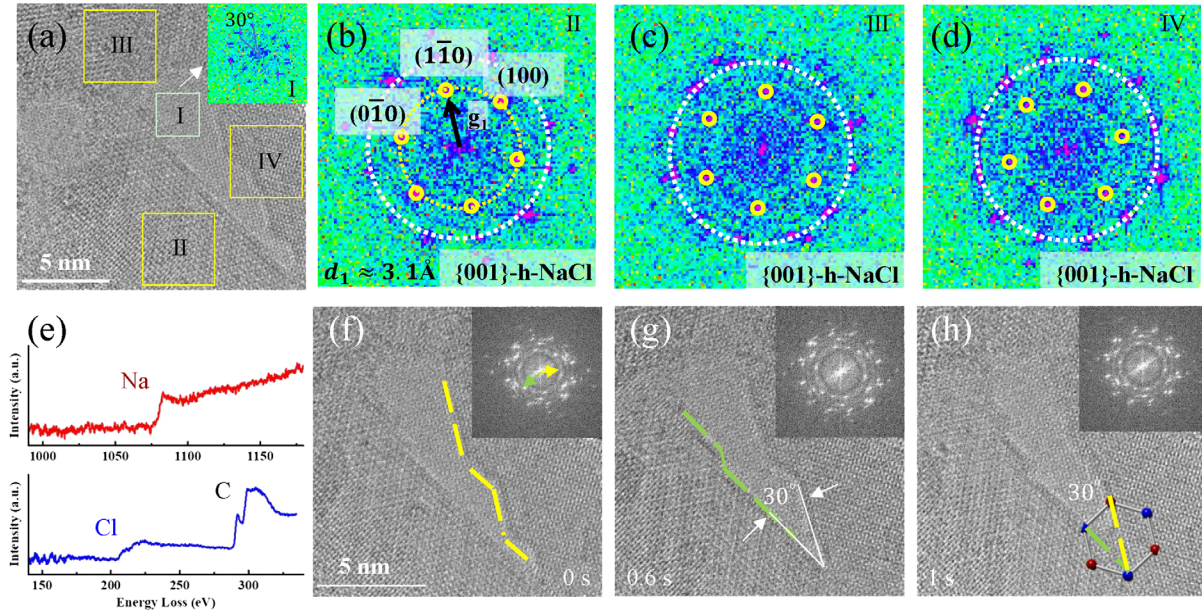
FIG. 2. Formation of the h-NaCl phase. (a) TEM image of NaCl crystals grown in a GLC, showing an in-plane hexagonal lattice. Inset: diffractogram of a graphene-only area with a rotation angle of approximately 30°. (b)–(d) The corresponding diffractograms of selected regions (yellow boxes) in (a), clearly showing sixfold symmetry (inner yellow circles). The rotation angles between NaCl and graphene (outer white dashed circle) varies. (e) EELS of the pocket area, showing signals only from C, Cl, and Na. (f)–(h) Sequential TEM images of h-NaCl crystal growth. The two predominant surfaces have an angle of 30°.

determine if the B1 crystallites have formed via a solid-to-solid transition, or if they have formed independently of h-NaCl. Thus, it remains an open question whether h-NaCl acts simply as an early—but ultimately unsuccessful—competitor of B1-NaCl (similar to recent observations in protein crystallization [41]), or if it acts as an intermediatory phase in a two-step mechanism [42]. The crystallization event shown in Fig. 3 typifies three out of the five events seen in our experiments (Videos 4–7). In the remaining two events, {110}-B1-NaCl is seen to form without the detection of h-NaCl, although we cannot preclude, e.g., the prior formation of a thin layer of h-NaCl. On balance, our results lean toward h-NaCl acting as an unsuccessful competitor to direct B1-NaCl formation,
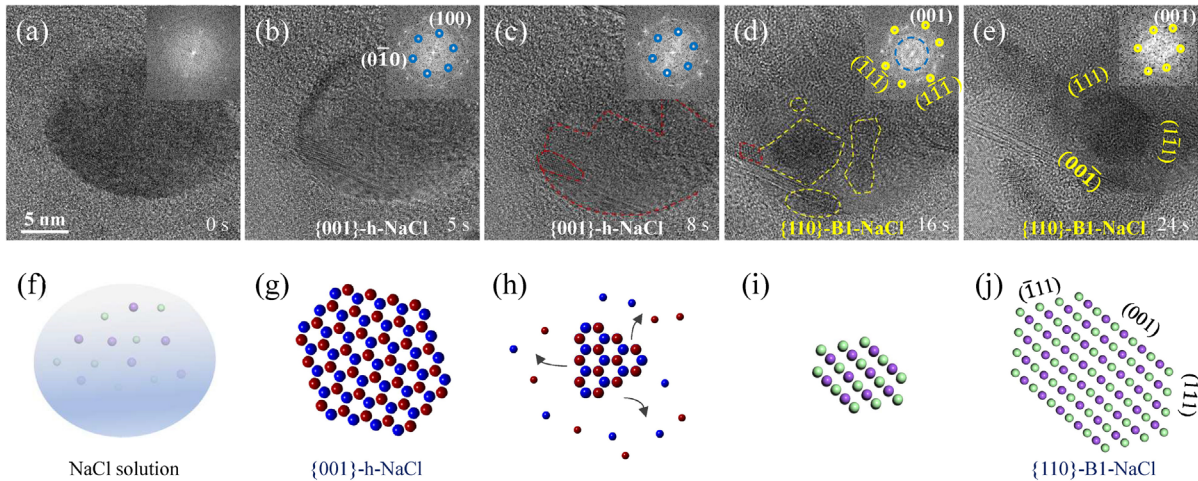

FIG. 3. Transformation from h-NaCl to {110}-B1-NaCl. (a)–(e) Sequential TEM images of a graphene pocket. Dark contrast in the middle of the image indicates the area of the trapped solution. Initially there is no crystal signal from the pocket [(a), inset]. After 5 s nuclei with the hexagonal structure fill the whole graphene pocket with a uniform lattice (b). Inset of (b) shows spots with sixfold symmetry. In the next stage the hexagonal structure shrinks (c), followed by transformation to B1-NaCl nuclei (d). Dashed red and yellow lines highlight the h-NaCl and B1-NaCl regions, respectively. Eventually, a large {110}-B1-NaCl crystal with a hexagonal shape is observed (e). (f)–(j) Schematics of the corresponding processes in (a)–(e).

though we cannot definitively rule out a two-step mechanism. In any case, it appears that the crystallization pathway is altered in a GLC environment, even qualitatively, from that in bulk solution.

Previous theoretical studies predict that h-NaCl is more stable than the B1 phase at large negative pressures, when it is a few layers thin, or when supported by a substrate [43–45]. Previous experimental studies have estimated high pressures (GPa) in GLCs. The fact that B1-NaCl (albeit with an exotic morphology) ultimately forms at the expense of h-NaCl suggests the former is stable while the latter is metastable. It therefore seems unlikely that pressure underlies the formation of h-NaCl. In order to further understand effects due to solvation and the interactions between the NaCl crystal and graphene, we have performed DFT calculations for three types of cluster, shown schematically in Figs. 4(a)–4(c): "{001}-B1" clusters, "{110}-B1" clusters, and "h clusters." In Fig. 4(d) we present calculated formation energies e_f per formula unit for different sized clusters. These calculations have been performed both in vacuum and with an implicit solvent model [46]. We see that the {001}-B1 clusters are significantly more stable than the {110}-B1 clusters in vacuum. In solution, however, the calculations with the implicit solvent model [25,30] suggest that the {110}-B1 clusters are marginally

more stable, which is also reflected in calculations with extended surfaces (Fig. S6). As these results have been obtained with an implicit solvent model we exercise caution, and simply take this as indicative that the difference in surface energies of {001} and {110} facets is greatly reduced in solution compared to their stark energy difference in vacuum. More importantly, we find that the {110}-B1 clusters interact much more favorably with graphene than do the {001}-B1 clusters, as shown in Fig. 4(e). This suggests that the formation of {110}-B1-NaCl nanocrystals (Fig. 1) may be driven by a combination solvation effects and a favorable interaction between {110} facets and graphene.

In Fig. 4(d) we also see that, while e_f for the bulk hexagonal crystal (dotted line) is far higher compared to that of the B1 structure (dashed line), the h-NaCl clusters are energetically similar to the B1 clusters. This is the case both in vacuum and with solvent. For very small cluster sizes of h-NaCl, its interaction with graphene [Fig. 4(e)] is comparable to the {110}-B1 clusters, though it becomes relatively less strong as size increases. During the initial stages of crystallization, we suggest the formation of the h-NaCl crystal is not disfavored on energetic grounds. As the crystal becomes larger, the preference for the B1 structure increases. These calculations are consistent with our experimental observation that the {110}-B1-NaCl nanocrystal ultimately forms.

There is increasing evidence that nucleation occurs nonclassically; notable experimentally observed examples include proteins [7], minerals [47], colloids [48], and polymeric solutions [1]. NaCl, a salt with a simple structure, is believed to follow CNT and shows cubic morphology. Our results suggest elements of nonclassical nucleation extend to NaCl, with the possibility of crystallization via an intermediate metastable crystalline phase: this appears to be distinct from the nonclassical mechanism reported at very high supersaturations [49]. More importantly, our results show that the crystallization pathway in solution can be engineered by the interaction between the crystallites and substrates, i.e., the unexpected transient formation of h-NaCl as a kinetic stable state in the nanosized capillaries, compared with the conventional cubic structure in the micron-sized open cell. In principle, this approach to achieve a nonclassical nucleation pathway could be readily extended to other systems [1,2,12].

Furthermore, in addition to the revealed crystallization mechanism, our findings clearly show that confinement in a GLC alters crystallization of NaCl both in terms of morphology and intermediate or transitory metastable phases without involving ultrahigh pressure. This opens up exciting possibilities in nanocrystal design; for example, the morphology controlling ability of the GLC could be useful for catalysis, where the catalytic behavior of a material sensitively depends on exposed facets [50]. Moreover, there has been growing interest in metastable
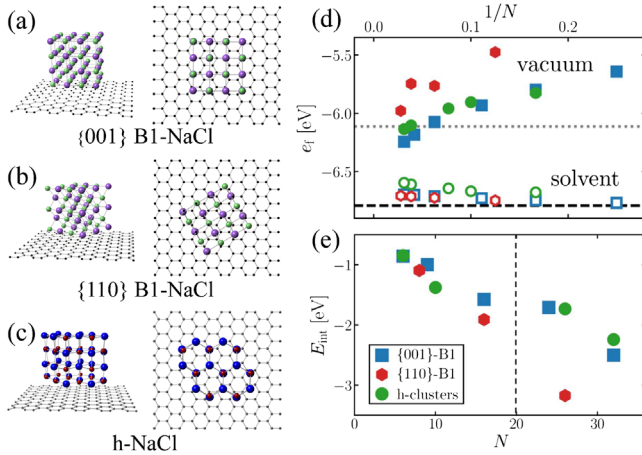

FIG. 4. Energetics of NaCl clusters. (a)–(c) Schematic representations of {001} B1, {110}-B1, and h clusters bound to graphene, as indicated at the bottom of each panel. (d) Formation energy per formula unit (e_f) vs $1/N$. In vacuum, {001}-B1 clusters (squares) are more stable than {110}-B1 clusters (hexagons) for finite N. In solvent, the two structures are energetically similar. While the bulk energy of the hexagonal structure (dotted line) is significantly higher than that of the B1 structure (dashed line), the energy difference is far less pronounced for h clusters (circles). (e) Interaction energies with graphene vs N. The {110}-B1 clusters interact much more favorably with graphene than do the {001}-B1 clusters. The vertical dashed line separates small clusters (all clusters interact with graphene similarly) and large clusters ({110}-B1 cluster interacts more strongly with graphene).

crystal structures of functional materials, including the III-V compound semiconductors and transition metal dichalcogenides [51,52]. Future studies may therefore use graphene-confined cells to grow these materials and to discover unknown metastable phases.

---

[*] L. W., J. C., and S. J. C. contributed equally to this work.
[†] wanglf@iphy.ac.cn;
[‡] sjc236@cam.ac.uk
[§] l_liu@pku.edu.cn
[‖] xdbai@iphy.ac.cn

[1] J. J. De Yoreo, P. U. Gilbert, N. A. Sommerdijk, R. L. Penn, S. Whitelam, D. Joester, H. Zhang, J. D. Rimer, A. Navrotsky, and J. F. Banfield, Science **349**, aaa6760 (2015).

[2] G. C. Sosso, J. Chen, S. J. Cox, M. Fitzner, P. Pedevilla, A. Zen, and A. Michaelides, Chem. Rev. **116**, 7078 (2016).

[3] D. Gebauer, M. Kellermeier, J. D. Gale, L. Bergström, and H. Cölfen, Chem. Soc. Rev. **43**, 2348 (2014).

[4] J. R. Cox, L. A. Ferris, and V. R. Thalladi, Angew. Chem. Int. Ed. **46**, 4333 (2007).

[5] W. D. Callister, Jr. and D. G. Rethwisch, *Fundamentals of Materials Science and Engineering: An Integrated Approach* (John Wiley & Sons, New York, 2020).

[6] C. Rodriguez-Navarro and L. G. Benning, Elements **9**, 203 (2013).

[7] A. Sauter, F. Roosen-Runge, F. Zhang, G. Lotze, R. M. Jacobs, and F. Schreiber, J. Am. Chem. Soc. **137**, 1485 (2015).

[8] M. H. Nielsen, S. Aloni, and J. J. De Yoreo, Science **345**, 1158 (2014).

[9] J. F. Lutsko, Sci. Adv. **5**, eaav7399 (2019).

[10] Y. Peng, F. Wang, Z. Wang, A. M. Alsayed, Z. Zhang, A. G. Yodh, and Y. Han, Nat. Mater. **14**, 101 (2015).

[11] Z. Ou, Z. Wang, B. Luo, E. Luijten, and Q. Chen, Nat. Mater. **19**, 450 (2020).

[12] V. J. Anderson and H. N. Lekkerkerker, Nature (London) **416**, 811 (2002).

[13] J. M. Yuk, J. Park, P. Ercius, K. Kim, D. J. Hellebusch, M. F. Crommie, J. Y. Lee, A. Zettl, and A. P. Alivisatos, Science **336**, 61 (2012).

[14] G. Algara-Siller, O. Lehtinen, F. Wang, R. Nair, U. Kaiser, H. Wu, A. Geim, and I. Grigorieva, Nature (London) **519**, 443 (2015).

[15] F. Corsetti, P. Matthews, and E. Artacho, Sci. Rep. **6**, 18651 (2016).

[16] J. Chen, G. Schusteritsch, C. J. Pickard, C. G. Salzmann, and A. Michaelides, Phys. Rev. Lett. **116**, 025501 (2016).

[17] A. Jabbarzadeh and X. Chen, Faraday Discuss. **204**, 307 (2017).

[18] A. Jabbarzadeh and B. Halfina, Nanoscale Adv. **1**, 4704 (2019).

[19] A. Cacciuto, S. Auer, and D. Frenkel, Nature (London) **428**, 404 (2004).

[20] Y. Su, G. Liu, B. Xie, D. Fu, and D. Wang, Acc. Chem. Res. **47**, 192 (2014).

[21] N. E. R. Zimmermann, B. Vorselaars, D. Quigley, and B. Peters, J. Am. Chem. Soc. **137**, 13352 (2015).

[22] N. Takayuki, S. Masaya, N. Hiroki, H. Koji, and N. Eiichi, J. Am. Chem. Soc. **143**, 1763 (2021).

[23] K. A. Tikhomirova, C. Tantardini, E. V. Sukhanova, Z. I. Popov, S. A. Evlashin, M. A. Tarkhov, V. L. Zhdanov, A. A. Dudin, A. R. Oganov, and D. G. Kvashnin, J. Phys. Chem. Lett. **11**, 3821 (2020).

[24] See Supplemental Material at http://link.aps.org/supplemental/10.1103/PhysRevLett.126.136001 for a discussion of the methods used as well as additional experimental and theoretical results, which includes Refs. [24–40].

[25] G. Kresse and J. Furthmüller, Phys. Rev. B **54**, 11169 (1996).

[26] S. Plimpton, J. Comput. Phys. **117**, 1 (1995).

[27] G. Kresse and D. Joubert, Phys. Rev. B **59**, 1758 (1999).

[28] J. Klimeš, D. R. Bowler, and A. Michaelides, J. Phys. Condens. Matter **22**, 022201 (2010).

[29] K. Mathew, V. S. C. Kolluru, and R. G. Hennig, VASPsol: Implicit solvation and electrolyte model for density-functional theory, GitHub, 2018, https://dx.doi.org/10.5281/zenodo.2555053.

[30] K. Mathew, R. Sundararaman, K. Letchworth-Weaver, T. A. Arias, and R. G. Hennig, J. Chem. Phys. **140**, 084106 (2014).

[31] I. S. Joung and T. E. Cheatham, J. Chem. Phys. B **112**, 9020 (2008).

[32] J. Klimeš, D. R. Bowler, and A. Michaelides, Phys. Rev. B **83**, 195131 (2011).

[33] H. J. C. Berendsen, J. R. Grigera, and T. P. Straatsma, J. Phys. Chem. **91**, 6269 (1987).

[34] G. J. Martyna, D. J. Tobias, and M. L. Klein, J. Chem. Phys. **101**, 4177 (1994).

[35] M. Parrinello and A. Rahman, J. Appl. Phys. **52**, 7182 (1981).

[36] W. Shinoda, M. Shiga, and M. Mikami, Phys. Rev. B **69**, 134103 (2004).

[37] M. E. Tuckerman, J. Alejandre, R. López-Rendón, A. L. Jochim, and G. J. Martyna, J. Phys. A **39**, 5629 (2006).

[38] R. W. Hockney and J. W. Eastwood, *Computer Simulation Using Particles* (Taylor & Francis, Inc., London, 1988).

[39] J. Kolafa and J. W. Perram, Mol. Simul. **9,** 351 (1992).

[40] H. C. Andersen, J. Comput. Phys. **52,** 24 (1983).

[41] T. Yamazaki, Y. Kimura, P. G. Vekilov, E. Furukawa, M. Shirai, H. Matsumoto, A. E. S. Van Driessche, and K. Tsukamoto, Proc. Natl. Acad. Sci. U.S.A. **114,** 2154 (2017).

[42] D. James, S. Beairsto, C. Hartt, O. Zavalov, I. Saika-Voivod, R. K. Bowles, and P. H. Poole, J. Chem. Phys. **150,** 074501 (2019).

[43] A. Kvashnin, E. Pashkin, B. Yakobson, and P. Sorokin, J. Phys. Chem. Lett. **7,** 2659 (2016).

[44] Ž. P. Čančarević, J. C. Schoen, and M. Jansen, Chem-Asian J. **3,** 561 (2008).

[45] A. G. Kvashnin, P. B. Sorokin, and D. Tománek, J. Phys. Chem. Lett. **5,** 4014 (2014).

[46] G. Kresse and J. Furthmüller, Phys. Rev. B **54,** 11169 (1996).

[47] F. C. Meldrum and R. P. Sear, Science **322,** 1802 (2008).

[48] N. D. Loh, S. Sen, M. Bosman, S. F. Tan, J. Zhong, C. A. Nijhuis, P. Král, P. Matsudaira, and U. Mirsaidov, Nat. Chem. **9,** 77 (2017).

[49] H. Jiang, P. G. Debenedetti, and A. Z. Panagiotopoulos, J. Chem. Phys. **150,** 124502 (2019).

[50] S. Selcuk and A. Selloni, Nat. Mater. **15,** 1107 (2016).

[51] Z. Y. Al Balushi, K. Wang, R. K. Ghosh, R. A. Vilá, S. M. Eichfeld, J. D. Caldwell, X. Qin, Y.-C. Lin, P. A. DeSario, and G. Stone, Nat. Mater. **15,** 1166 (2016).

[52] T.-R. T. Han, F. Zhou, C. D. Malliakas, P. M. Duxbury, S. D. Mahanti, M. G. Kanatzidis, and C.-Y. Ruan, Sci. Adv. **1,** e1400173 (2015).